

Quantum State-Resolved Study of the Four-Atom Reaction $\text{OH}^- (\text{X}^1\Sigma^+) + \text{D}_2 (\text{X}^1\Sigma_g^+, \nu = 0) \rightarrow \text{HOD} (\text{X}^1\text{A}', \nu') + \text{D}^- ({}^1\text{S})$

Yue Li, Li Liu, and James M. Farrar*

Department of Chemistry, University of Rochester, Rochester, New York 14627

Received: May 10, 2005; In Final Form: June 15, 2005

The D^+ transfer reaction between $\text{OH}^- (\text{X}^1\Sigma^+)$ and D_2 was studied with crossed molecular beam experiments and quantum chemical calculations at collision energies of 89 and 68 kJ/mol. The D^- product ions were observed and measured for the first time in the crossed beam experiments. The center-of-mass (c.m.) flux distributions of the D^- product ions exhibit significant asymmetry, and their maxima are close to the velocity and direction of the precursor D_2 beam. The data are consistent with a direct mechanism that occurs on a time scale significantly less than a rotational period of the transient complex formed by approaching reactants. The D^+ transfer results primarily in the excitation of the H–O–D bending vibrational mode of the molecular product. The experimental observation is in agreement with theoretical results showing that, during the D^+ transfer, the H–O–D bond angle changes significantly.

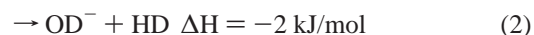
Investigations of chemical reaction dynamics seek to understand how the forces that approaching reactants and separating products exert on one another control disposal of the available energy among product degrees of freedom. The crossed molecular beam technique and high-level theoretical calculations have been demonstrated to provide high-resolution information on reaction mechanisms and energy disposal. However, detailed state-to-state measurements and complementary calculations have been limited to three-atom systems such as $\text{H} + \text{D}_2$,¹ $\text{F} + \text{H}_2$,² and $\text{O} + \text{H}_2$,³ in which the small number of electrons and rovibrational degrees of freedom make such studies tractable. Recently, these efforts have also been extended to four-atom systems, $\text{AB} + \text{CD} \rightarrow \text{ABC} + \text{D}$ or $\text{A} + \text{BCD} \rightarrow \text{AB} + \text{CD}$, to achieve a comparable understanding for systems with up to six product internal degrees of freedom. Among them, the combustion and atmospheric reaction $\text{OH} + \text{H}_2 \rightarrow \text{H}_2\text{O} + \text{H}$ ($\Delta H = -63$ kJ/mol) is an important benchmark reaction for both theoretical^{4–6} and experimental^{7–9} studies. Recently, experimental and theoretical results on this system have been reviewed by Smith and Crim.¹⁰

The state of knowledge of the dynamics of ion–molecule reactions generally parallels that of neutral systems, although the detailed level of experimental and theoretical insight is significantly lower. Among triatomic systems, the $\text{H}^- + \text{H}_2$ system has been subjected to high-resolution experimental^{11–13} and theoretical methods.¹⁴ However, the state of knowledge of four-atom ionic systems is significantly less well-developed than that for neutrals. The anion–neutral reaction between OH^- and H_2 serves as an example. The collision complex of the reaction, H_3O^- , has been proven to be a stable species¹⁵ and serves as a model for negative ion–water complexes. The $\text{OH}^- + \text{H}_2 \rightarrow \text{H}_2\text{O} + \text{H}^-$ reaction is the simplest proton transfer reaction involving H_2O . The reverse reaction of the reaction is also the first example reported of a negative ion–molecule reaction.¹⁶

Thus, H_3O^- has attracted the attention of many theorists^{17–23} and experimentalists.^{9,24,25}

In this paper, we report both experimental and theoretical studies of the proton transfer reaction of $\text{OH}^- + \text{H}_2$, using the isotopically labeled system $\text{OH}^- + \text{D}_2$. To provide insight into key reactive intermediates that influence this reaction, we have calculated the structures, vibrational frequencies, and energies of the relevant intermediates in the $\text{OH}^- + \text{D}_2$ reaction at the B3LYP/6-311++G (d,p) and CCSD(T)/6-311++G (d,p) levels of theory using the Gaussian 98 program package.²⁶ The results obtained with both methods agree well with each other and compare well with other theoretical results.^{17–19,21} The structures and energy diagram obtained at the CCSD(T) level are shown in Figure 1. The H_3O^- ion has three isomers: $\text{H}_2\text{O}\cdot\text{H}^-$, $\text{OH}\cdot\text{H}_2^-$, and pyramidal H_3O^- . $\text{H}_2\text{O}\cdot\text{H}^-$ is about 10 kJ/mol more stable than $\text{OH}\cdot\text{H}_2^-$, while pyramidal H_3O^- , considered as a “double Rydberg” isomer, has an energy of 160 kJ/mol higher than the other two structures. Thus, it is not taken into account in the mechanistic discussions of this study. In a photoelectron spectroscopy study⁹ of H_3O^- , it was found that the two forms of the ion, $\text{H}_2\text{O}\cdot\text{H}^-$ and $\text{OH}^- \cdot \text{H}_2$, can interconvert. Photodetachment spectroscopy was thus used to study the transition state region of the reaction $\text{OH} + \text{H}_2 \rightarrow \text{H}_2\text{O} + \text{H}$. The photodetachment of $\text{H}_3\text{O}^- (\nu = 0, \text{H}_2\text{O}\cdot\text{H}^-)$ probes the $\text{H}^- + \text{H}_2\text{O}$ exit valley, while that of $\text{H}_3\text{O}^- (\nu = 2, \text{OH}^- \cdot \text{H}_2)$ probes the transition state and entrance valley of the above reaction.

The three possible product channels and reaction exothermicities of the $\text{OH}^- + \text{D}_2$ reaction are as follows.



Experimentally, several groups^{27–31} have studied the reactions between OH^- and H_2 (or their isotopic analogues), focusing on

* To whom correspondence should be addressed. E-mail: farrar@chem.rochester.edu.

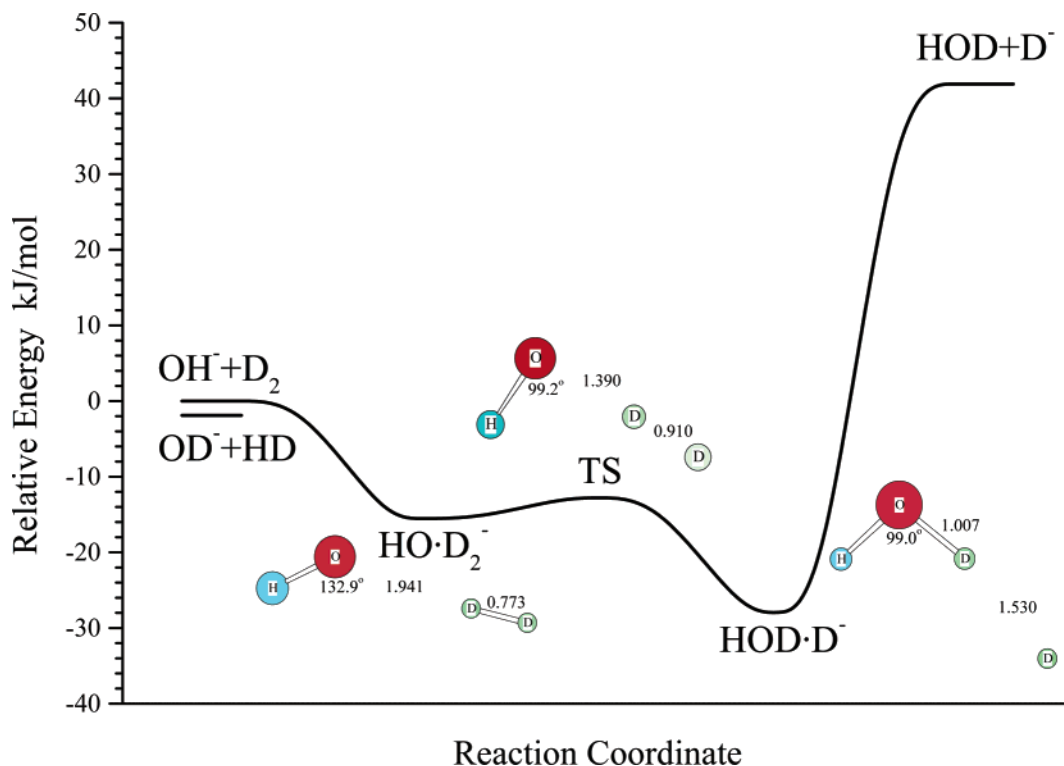


Figure 1. Schematic energy diagram obtained from CCSD(T) calculations for the $\text{OH}^- + \text{D}_2$ reaction. The structure parameters are in angstroms and degrees.

the H–D isotope exchange reaction (channel 2). So far, no experimental results have been reported on the proton (deuteron) transfer reaction to form H^- (or D^-). The production of H^- is an endothermic process and is expected to have a lower reaction cross section at threshold than the other two channels. This fact, in conjunction with unfavorable kinematics for light particle detection in a crossed beam experiment, may contribute to this lack of experimental data for H^- (or D^-) product formation. Experimental data from our laboratory show that, at a collision energy of 42 kJ/mol (threshold energy of channel 3), the branching ratio of the three products, $\text{D}^-/\text{OD}^-/\text{OH}^-$, is approximately 1:12:50. However, with increasing collision energy, the latter two channels are significantly suppressed and the D^- channel becomes dominant. This letter reports the first experimental results for the formation of D^- .

In this study, the OH^- ($X^1\Sigma^+$) ions were produced by electron impact on a room temperature gaseous mixture of 5% NH_3 (99.99% purity) in N_2O (99.6% purity). Reactant OH^- ions are produced in the electron impact region by the ion–molecule reaction of O^- with NH_3 , whose exothermicity of -11 kJ/mol prohibits the formation of excited vibrational states. The ions are mass-selected with a 60° magnetic sector. After deceleration to the desired beam energy, the ion beam, with laboratory energies of 406 and 318 kJ/mol in these experiments, has a full width at half-maximum (fwhm) laboratory energy distribution of about 24 kJ/mol. The corresponding center-of-mass (c.m.) energies are 89 and 68 kJ/mol, with a fwhm barycentric energy spread of 5 kJ/mol. The neutral beam, formed by supersonic expansion of the pure deuterium gas through a 0.07 mm nozzle, intersects with the ion beam at 90° . A tuning fork chopper modulates the beam at 30 Hz to provide the time synchronization for the experiment. A rotatable electrostatic energy analyzer with a laboratory resolution of 7 kJ/mol was used to measure the kinetic energy distributions of the reactant and product ions. The product ions were mass-analyzed with a quadrupole mass spectrometer and detected with a dual microchannel plate ion

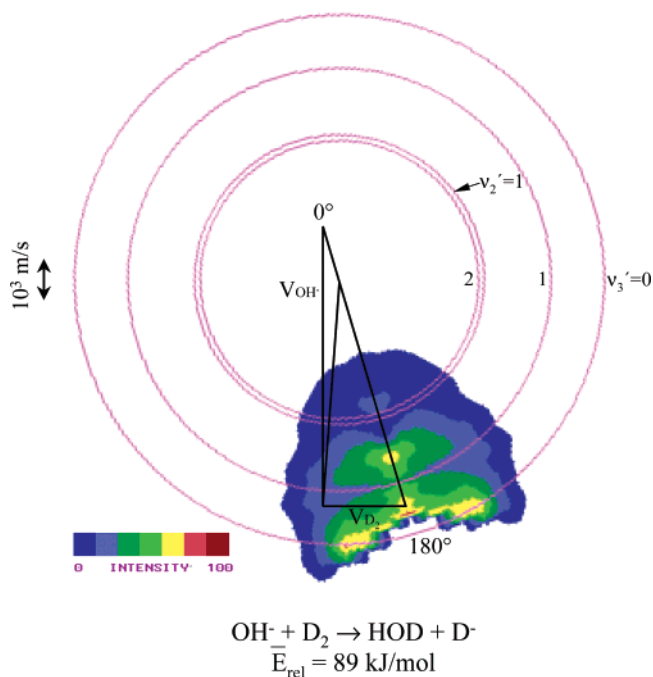


Figure 2. Newton diagram and scattered product flux contour map at a collision energy of 89 kJ/mol. The circles correspond to the velocity space loci of products formed with a selected number of quanta in the H–O–D bending mode (ν_3') or the O–D stretch (ν_2').

detector. Data were collected with a computer-controlled multichannel scalar synchronized with the beam modulation.

The kinetic energy distributions of the scattered product ions were measured at 22 fixed laboratory angles. The energy distributions were then normalized by angular distributions of product ions. The experimental intensities measured in the laboratory coordinate system at a particular laboratory velocity, v , and scattering angle, Θ , represent a convolution of the reactant velocity distributions, $f_i(\mathbf{v}_i)$, with the c.m. cross section for the

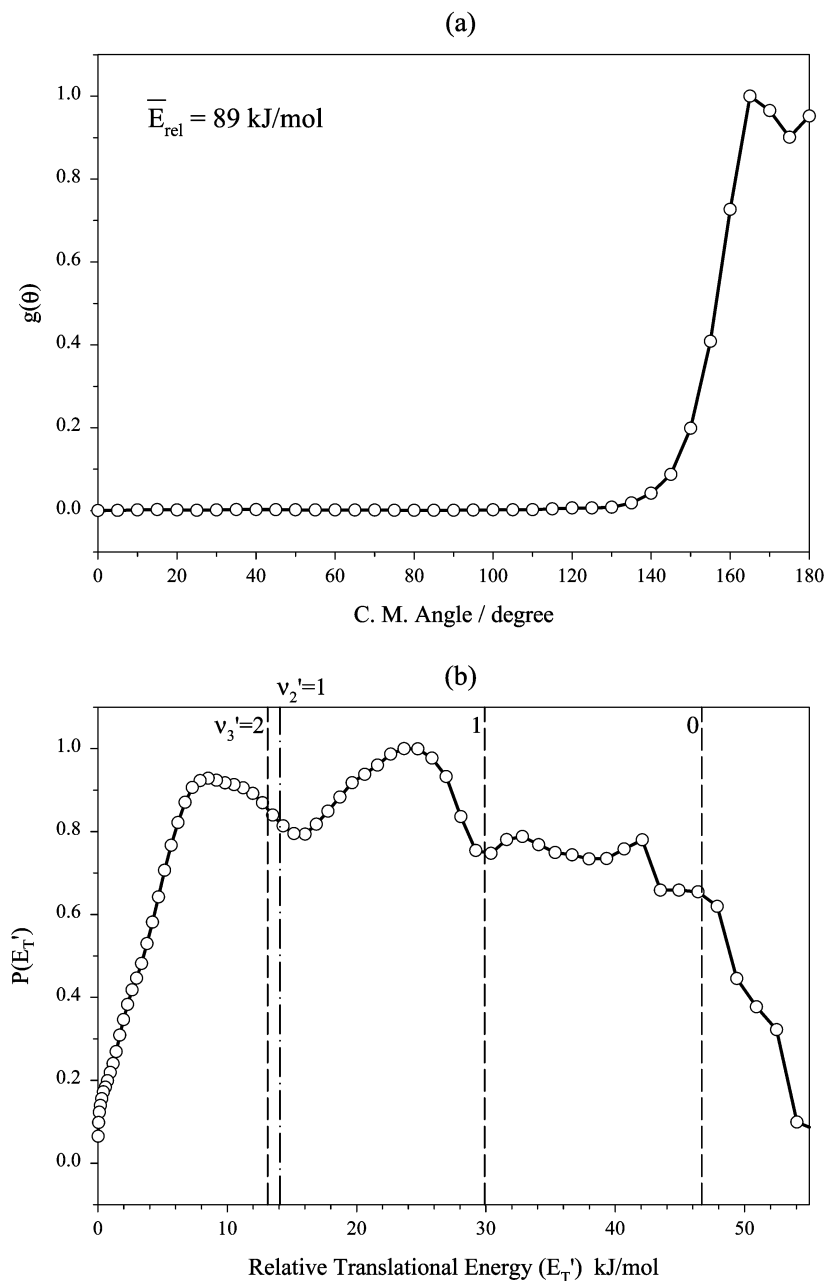


Figure 3. (a) Angular distributions; (b) relative translational energy distribution of the product D^- ions in c.m. coordinates at a collision energy of 89 kJ/mol. The vertical dashed lines correspond to the energies for the formation of rotationally cold products with specified numbers of vibrational quanta.

formation of product quantum state n summed over energetically accessible product quantum states, as indicated in eq 4. The c.m. cross section, $I_{\text{c.m.}}(\mathbf{u}_n, \theta; V_{\text{rel}})$, is recovered numerically from eq 4 using the iterative deconvolution method of Siska.³²

$$I_{\text{lab}}(\mathbf{v}, \Theta) = v^2 \int_0^\infty d\mathbf{v}_2 f_2(\mathbf{v}_2) \int_0^\infty d\mathbf{v}_1 f_1(\mathbf{v}_1) \frac{V_{\text{rel}}}{u^2} \sum_n I_{\text{c.m.}}(\mathbf{u}_n, \theta; V_{\text{rel}}) \delta(\mathbf{u} - \mathbf{u}_n) \quad (4)$$

Application of this deconvolution procedure produces c.m. cross sections that, when transformed back to the laboratory frame with appropriate averaging over experimental velocity distributions and beam intersection angles, recover the experimental data with a standard deviation of <10%.

Figure 2 shows the reaction product flux contour map in polar coordinates, superimposed on the Newton kinematic diagram

at a collision energy of 89 kJ/mol. The angular and energy distributions are shown in Figure 3. The figures show that, at this collision energy, the product D^- ions are distributed at large angles, close to the direction of the precursor D_2 reactants. According to linear momentum conservation, its neutral partner, HOD, is forward scattered with respect to the direction of the primary ion beam, OH^- . This behavior is characteristic of a direct reaction that proceeds via large impact parameters. A similar result is also observed at the lower energy, 68 kJ/mol, as shown in Figure 4. The appearance of a high-energy tail beyond the thermochemical limit arises primarily from incomplete deconvolution of the data, exacerbated by the fact that these products have near-thermal laboratory energies. The asymmetric distributions indicate that the reaction intermediate, D_2HO^- , must be short-lived relative to its rotational period (<4 ps). The product ion is monoatomic, and its translational energy distributions encode the internal energy distributions of the HOD

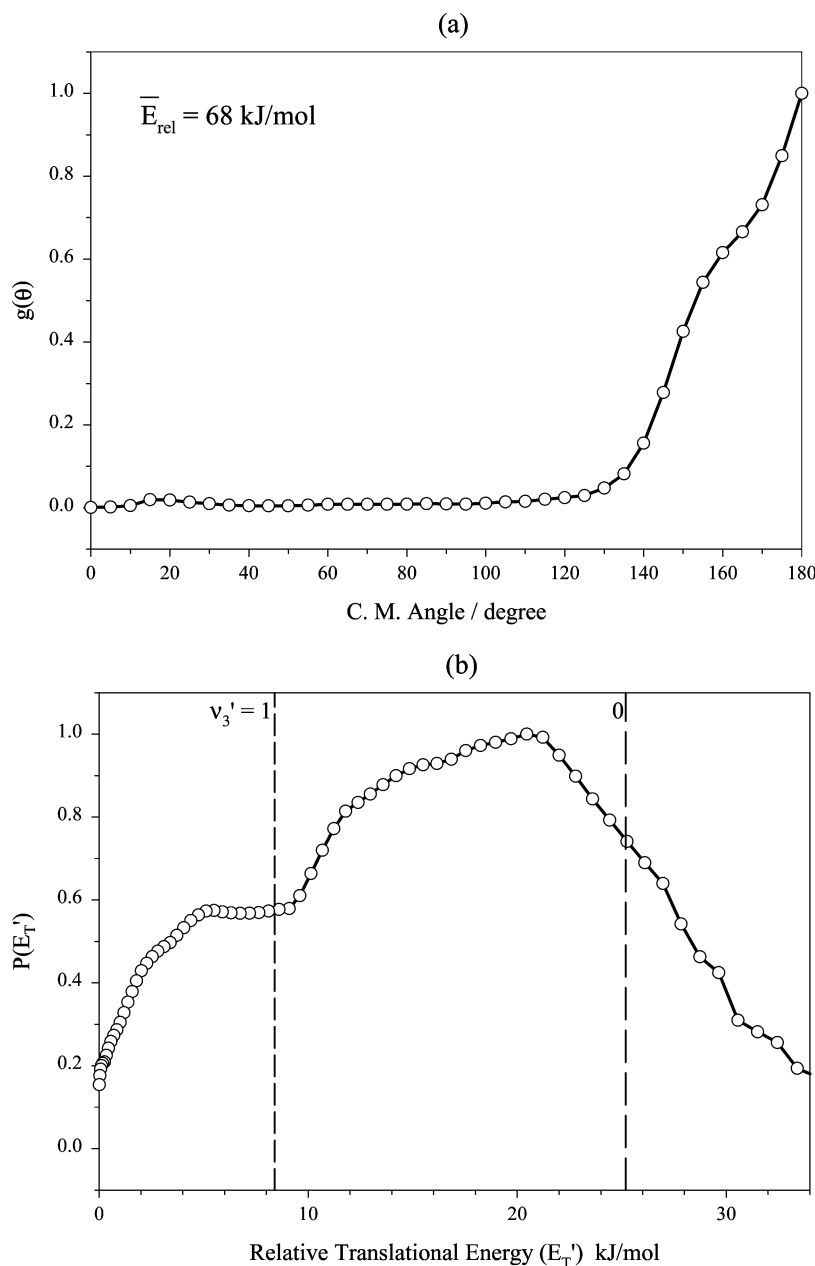


Figure 4. (a) Angular distribution; (b) relative translational energy distribution of the product D^- ions in c.m. coordinates at a collision energy of 68 kJ/mol. The vertical dashed lines correspond to the energies for the formation of rotationally cold products with specified numbers of vibrational quanta.

products with high kinematic dispersion. In Figures 2 and 3b, three vibrational band structures with an energy spacing of 17 kJ/mol can be clearly resolved. The three vibrational mode frequencies of HOD are 3707 (44.3 kJ/mol, O–H stretching), 2727 (32.6 kJ/mol, O–D stretching), and 1402 cm^{-1} (16.8 kJ/mol, H–O–D bending), respectively. We thus assign the vibrational structures as the excitation of the H–O–D bending mode. The O–D stretching frequency is approximately twice that of H–O–D bending and cannot be distinguished from the $\nu' = 2$ excitation of the latter in this study. Similarly, two vibrational structures can also be observed in Figure 4. According to Figures 3 and 4, the relative populations of the vibrational states are approximately 3:3:2 (corresponding to vibrational quantum number $\nu' = 0, 1, 2$) at 89 kJ/mol and 4:1 ($\nu' = 0, 1$) at 68 kJ/mol. We cannot rule out the possibility that, at the higher collision energy, some of the products that we assign two quanta of H–O–D bending may instead have energy in the first excited O–D stretching mode. For the two

collision energies, the corresponding available total energies are 47 and 26 kJ/mol, respectively. From Figures 3 and 4, the product average translational energies are 27 and 18 kJ/mol; that is, 57 and 69% of the total energies are converted to the translational energies of the products, respectively. Therefore, as the collision energy increases, an increasing fraction of the excess translational energy of the approaching reactants is converted into the internal energy of the products.

The internal energy distributions of the products provide important insight into the roles of the intermediate complexes and the exit channel effects that arise as the products are formed. Figure 1 shows that, in the initial electrostatic complex formed as OH^- approaches D_2 , the incipient H–O–D angle is approximately 133° , significantly distorted from the equilibrium angle in the isolated HOD molecule. The transition state separating this encounter complex from the electrostatic $\text{HOD}\cdot\text{D}^-$ complex that leads to products is characterized by an incipient bond angle of 99° , much closer to the value in the free product.

This decrease in bending angle suggests that the bending mode can be excited in this complex. A significant shortening of the nascent O–D bond, from 1.39 to 1.01 Å, also suggests that the O–D stretching vibration in HOD may be excited. However, as we have discussed previously, we cannot distinguish between products with internal energies equivalent to the first overtone of the H–O–D bend and the fundamental of the O–D stretch; the low population of products with this amount of internal excitation argues against any selectivity in populating the O–D stretch. The endothermicity of the D–D bond cleavage and its associated late transition state evidently do not play a role in establishing energy disposal in this reaction. The energy that must be supplied to reach the products from the HOD•D⁻ complex is only 16% of the bond energy in D₂. Coupled with the fact that the transition state for the reverse association reaction to form the complex is loose, it is not surprising that exit channel effects are minimal and that the significant changes in geometry occurring in passing through the region marked “TS” in Figure 1 are critical in determining the disposal of energy. The data shown in Figure 4 also indicate the presence of rotational excitation in the reaction products, with most probable values, calculated from the displacements of the peaks from the vibrational thresholds, corresponding to 5 kJ/mol for $v' = 0$ and 3 kJ/mol for $v' = 1$. Because of the widths of the kinetic energy distributions, the uncertainties in these numbers are large.

This result contrasts with those reported for the corresponding neutral system $\text{OH} + \text{D}_2 \rightarrow \text{HOD} + \text{D}$ by Stratisar et al.⁷ In this system, which is exothermic by 63 kJ/mol, the dynamics are governed by an early transition state in which energy is released as the reactants approach, resulting in an extended O–D bond that leads to products with significant amounts of vibrational excitation in the O–D stretch. At a collision energy of 28 kJ/mol, that study demonstrated that only 37% of the total available energy went into translation, with the balance deposited into excitation of the stretching mode in the newly formed OD bond. Their results are in good agreement with the theoretical calculation results that the OD bond is significantly longer in the transition state than in the HOD product.

Experimental data such as those presented here provide significant challenges to theory. The foundation provided by benchmark calculations and experiments on three- and four-atom systems will ultimately lead to predictive models for more complex systems, including plasma chemistry and reactive ion etching environments. It is our hope that the present results on this prototypical four-atom ionic system will enhance our knowledge of low-energy reactive ion processes in the same way that the analogous neutral system has provided benchmark data for theory.

References and Notes

- (1) Schnieder, L.; Seekamp-Rahn, K.; Borkowski, J.; Wrede, E.; Welge, K. H.; Aoi, F. J.; Banares, L.; D'Mello, M. J.; Herrero, V. *J. Science* **1995**, *269*, 207–210.
- (2) Manolopoulos, D. E.; Stark, K.; Werner, H.-J.; Arnold, D. W.; Bradforth, S. E.; Neumark, D. M. *Science* **1993**, *262*, 1852–1855.
- (3) Liu, X.; Lin, J. J.; Harich, S.; Schatz, G. C.; Yang, X. *Science* **2000**, *289*, 1536–1538.
- (4) Defazio, P.; Gray, S. K. *J. Phys. Chem. A* **2003**, *107*, 7132–7137.
- (5) Zhang, D. H.; Yang, M.; Lee, S. *J. Chem. Phys.* **2002**, *116*, 2388–2394.
- (6) Zhang, Y.; Zhang, D.; Li, W.; Zhang, Q.; Wang, D.; Zhang, D. H.; Zhang, J. Z. H. *J. Phys. Chem.* **1995**, *99*, 16824–16828.
- (7) Stratisar, B. R.; Lin, C.; Davis, H. F. *Science* **2000**, *290*, 958–961.
- (8) Alagia, M.; Balucani, N.; Casavecchia, P.; Stranges, D.; Volpi, G. *J. Chem. Phys.* **1993**, *98*, 2459–2462.
- (9) de Beer, E.; Kim, E. H.; Neumark, D. M.; Gunion, R. F.; Lineberger, W. C. *J. Phys. Chem.* **1995**, *99*, 13627–13636.
- (10) Smith, I. W. M.; Crim, F. F. *Phys. Chem. Chem. Phys.* **2002**, *4*, 3543–3551.
- (11) Zimmer, M.; Linder, F. *J. Phys. B: At. Mol. Opt. Phys.* **1995**, *28*, 2671–2687.
- (12) Zimmer, M.; Linder, F. *Chem. Phys. Lett.* **1992**, *195*, 153–158.
- (13) Haufler, E.; Schlemmer, S.; Gerlich, D. *J. Phys. Chem. A* **1997**, *101*, 6441–6447.
- (14) Panda, A. N.; Giri, K.; Sathyamurthy, N. *J. Phys. Chem. A* **2005**, *109*, 2057–2061.
- (15) Kleingeld, J. C.; Nibbering, N. M. M. *Int. J. Mass Spectrom. Ion Phys.* **1983**, *49*, 311–318.
- (16) Muschlitz, E. E. J. *J. Appl. Phys.* **1957**, *28*, 1414–1418.
- (17) Chalasinski, G.; Kendall, R. A.; Simons, J. *J. Chem. Phys.* **1987**, *87*, 2965–2975.
- (18) Cremer, D.; Kraka, E. *J. Phys. Chem.* **1986**, *90*, 33–40.
- (19) Wang, D.; Zhang, J. Z. H.; Yu, C.-h. *Chem. Phys. Lett.* **1997**, *273*, 171–178.
- (20) Xantheas, S. S.; Dunning, T. H., Jr. *J. Phys. Chem.* **1992**, *96*, 7505–7506.
- (21) Ortiz, J. V. *J. Chem. Phys.* **1989**, *91*, 7024–7029.
- (22) Thompson, W. H.; Karlsson, H. O.; Miller, W. H. *J. Chem. Phys.* **1996**, *105*, 5387–5396.
- (23) Thompson, W. H.; Miller, W. H. *J. Chem. Phys.* **1994**, *101*, 8620–8627.
- (24) Miller, T. M.; Viggiano, A. A.; Stevens Miller, A. E.; Morris, R. A.; Henchman, M.; Paulson, J. F. *J. Chem. Phys.* **1994**, *100*, 5706–5714.
- (25) Lange, W. D.; Nibbering, N. M. M. *Int. J. Mass Spectrom. Ion Processes* **1987**, *80*, 201–209.
- (26) Frisch, M. J.; Trucks, G. W.; Schlegel, H. B.; et al. *Gaussian 98*, revision A.11.1; Gaussian, Inc.: Pittsburgh, PA, 2001.
- (27) Grabowski, J. J.; DePuy, C. H.; Bierbaum, V. M. *J. Am. Chem. Soc.* **1983**, *105*, 2565–2571.
- (28) Henchman, M.; Paulson, J. F. *Radiat. Phys. Chem.* **1988**, *32*, 417–423.
- (29) Viggiano, A. A.; Morris, R. A. *J. Chem. Phys.* **1994**, *100*, 2748–2753.
- (30) Meot-Ner, M.; Lloyd, J. R.; Hunter, E. P.; Agosta, W. A.; Field, F. H. *J. Am. Chem. Soc.* **1980**, *102*, 4672–4676.
- (31) Lee, S. T.; Farrar, J. M. *J. Chem. Phys.* **2000**, *113*, 581–595.
- (32) Siska, P. E. *J. Chem. Phys.* **1973**, *59*, 6052–6060.